The interaction of PRC2 with RNA or chromatin is mutually antagonistic

Manuel Beltran, Christopher M. Yates, Lenka Skalska, Marcus Dawson, Filipa P. Reis, Keijo Viiri, Cynthia L. Fisher, Christopher R. Sibley, Benjamin M. Foster, Till Bartke, Jernej Ule and Richard G. Jenner

SUPPLEMENTAL FIGURES

Supplemental Figure S1. Co-precipitation of SUZ12 and EZH2 by CLIP and PAR-CLIP.

A. SDS-PAGE for RNPs enriched by CLIP for endogenous SUZ12 (left) or EZH2 (right) in WT mouse ESC. CLIP was performed with and without UV crosslinking. The autoradiogram is shown at the top and the corresponding SUZ12 and EZH2 immunoblots below.

B. Suz12 CLIP autoradiogram and immunoblots after washes including 5 M Urea. EZH2 is still co-precipitated.

C. PAR-CLIP for SUZ12 and EZH2 in the presence and absence of 2% lauryl-dimethylbetaine in the lysis and IP buffers. 2% lauryl-dimethylbetaine was previously suggested to separate EZH2 from SUZ12 (Kaneko et al., 2013).

D. PAR-CLIP for SUZ12 in WT and *Suz12*$^{-/-}$ mES cells with and without 4-sU, 365 nm UV and T4-PNK and with increasing concentrations of RNase T_1 (10^5, $2x10^5$, $4 x10^5$, 10^6 U/ml).

E. Autoradiogram and immunoblot of the SUZ12 and EZH2 RNPs after RNase I or DNase I overdigestion, confirming that the radioactive smear is RNA and not DNA.

F. iCLIP for EZH2 with two different antibodies, AC22 (kinds gift from Adrian Bracken) and D2C9 (Cell Signalling) in *Ezh2*$^{fl/fl}$ and *Ezh2*$^{\Delta/\Delta}$ cells. EZH2 immunoblots are shown below. Neither antibody precipitated a radiolabelled RNP in an EZH2-dependent manner.

G. Immunofluoresence microscopy for Hoechst and GFP in *Ezh2*$^{fl/fl}$-GFP and *Suz12*$^{-/-}$-GFP cell lines. *Ezh2*$^{fl/fl}$-GFP cells were used for iCLIP and UV-RIP (Supplemental Fig. S4C and D), *Suz12*$^{-/-}$-GFP cells for UV-RIP.

Supplemental Figure S2. Purified RNA and iCLIP library construction.

A. Autoradiograms of each sequenced CLIP. The region of gel isolated for RNA purification is marked by a red box. PRC2-RNPs 10-30 kDa above the size of SUZ12/EZH2 were isolated, as is

standard for iCLIP. The size-shift is due to crosslinking of the proteins to RNA trimmed to different lengths by the RNase treatment. The size markers are indicated to the left of each gel.

B. TBE-gel electrophoresis of libraries generated from the top, high, medium and low cDNA fractions (see Konig et al. 2010; Huppertz et al. 2014). The number of PCR cycles used to generate each library is indicated above and the size markers to the left.

C. iCLIP autoradiograms for SUZ12 in UV-crosslinked or non-crosslinked cells. The gel regions isolated for RNA purification are marked by red boxes. The size markers are indicated between the two lanes.

D. Test PCR amplifications to gauge the minimum cycle number required to generate libraries (performed in order to minimise sequence reads from PCR duplicates (Konig et al. 2010; Huppertz et al. 2014)). 23 cycles were required to amplify cDNA from SUZ12 iCLIP in UV-crosslinked cells and 36 cycles for non-crosslinked cells (13 extra cycles, meaning 2^{13} or 8192-fold fewer template cDNA molecules).

E. TBE-gel electrophoresis of the final libraries generated from the different size cDNA fractions. The number of PCR cycles used to generate each library is indicated above and the size markers to the left. The libraries generated from non-crosslinked cells do not exhibit the expected sizes and are instead mostly adapters, indicative of PCR artefacts.

Supplemental Figure S3. iCLIP for PRC2, FUS and HNRNPC.

A. Scatter plot of significant crosslinks per gene (RPKM – crosslinks per kilobase per million total reads) for PRC2 in WT (*Ezh2*$^{fl/fl}$) cells versus *Suz12*$^{-/-}$ cells. The two iCLIP experiments (WT replicate 6 and *Suz12*$^{-/-}$ replicate 2) were performed in parallel with the same UV energy and with equal numbers of cells.

B. PRC2 crosslinking at the genes *Phf17, Rbpj and Fgf4*. Details as for Figure 1B.

Supplemental Figure S4. Promiscuous RNA binding by PRC2.

A. Average chromatin-binding profiles (reads/million) of RNA polymerase II (-input) and H3K4me3 (vs H3) at the TSS of genes with significant PRC2 RNA crosslinks and those without.

B. PRC2, FUS and HNRNPC RNA crosslinks across the RNA sequence of *CreERT2*, expressed in *Ezh2*$^{fl/fl}$ cells.

C. Enrichment of GFP RNA relative to input by UV-RIP for SUZ12 in *Ezh2*$^{fl/fl}$-GFP and *Suz12*$^{-/-}$-GFP cells, with and without UV crosslinking.

D. Amounts of GFP RNA (top) or unspliced *Srsf1* RNA (bottom) relative to input by UV-RIP for SUZ12 in *Ezh2*$^{fl/fl}$-GFP cells or in *Ezh2*$^{fl/fl}$ cells. *Ezh2*$^{fl/fl}$ cell lysate was either left untreated or spiked with *in vitro* transcribed GFP RNA prior to SUZ12 IP. 5, 0.5 or 0.05 μg of GFP RNA were spiked in, equivalent to 36,000, 3,600 and 360 RNA copies per cell, respectively. The amount of GFP RNA measured in the IP and whole cell extract (WCE) for each sample is shown relative to the crosslinked *Ezh2*$^{fl/fl}$-GFP input to allow comparison of GFP RNA concentrations between samples (0.1% of each input served as WCE in the qPCR). Unlike *in vivo* expressed GFP RNA, crosslinked to PRC2 by UV irradiation, spiked-in GFP RNA is not precipitated with PRC2. *Srsf1* was chosen as a representative endogenous RNA control.

E. Scatter plots showing gene length (kb) and nuclear RNA abundance (reads) for all genes (black), genes with significant FUS crosslinks (blue, left) or HNRNPC crosslinks (green, right) and genes previously identified to produce PRC2-binding ezRNAs (cyan; Kaneko et al. 2013).

F. Average crosslink profiles (reads/million) for PRC2 from iCLIP for SUZ12 (red) and PAR-CLIP for EZH2 (blue, Kaneko et al. 2013). Genes are divided into those with significant PRC2 iCLIP crosslinks and defined as ezRNA positive by Kaneko and colleagues and those with significant PRC2 iCLIP crosslinks and defined as ezRNA negative by Kaneko et al. 2013. Nuclear RNA-seq read densities are shown below for comparison. Both methods report the same RNA crosslink profile for both sets of genes, albeit iCLIP is able to detect PRC2 RNA crosslinking at genes with lower expression levels.

G. SDS-PAGE for RNPs enriched by CLIP for MYC-EED in *Eed4* cKO cells before or after addition of doxycycline to repress expression of MYC-EED4. The autoradiogram is shown at the top and the corresponding SUZ12, EZH2 and MYC-EED immunoblots below. CLIP was performed with and without UV crosslinking and T4-polynucleotide kinase (T4-PNK) and with increasing concentrations of RNase I (1, 4 & 10 U/ml). The position of the SUZ12/EZH2 RNP from which RNA was sequenced (Supplemental Fig. 4H) is marked by an arrow.

H. Average RNA crosslinking profiles across all genes for SUZ12/EZH2 when co-precipitated by MYC-EED (see G.).

I. Scatter plots of nuclear RNA abundance (RPKM) against FUS (left) or HNRNPC (right) crosslink density (RPKM). Genes marked in red are significantly enriched for PRC2 crosslinks

compared to nuclear RNA abundance (FDR<0.05; see Fig. 2E) and are also enriched for FUS and HNRNPC crosslinks.

Supplemental Figure S5. Characterisation of *Ezh2*$^{\Delta/\Delta}$ and *Jarid2*$^{-/-}$ cells.

A. Left: Immunoblotting for SUZ12, EZH2, JARID2, H3K27me3 and H3 in *Ezh2*$^{fl/fl}$ cells before and 4 days after the addition of tamoxifen to induce deletion of the EZH2 SET domain (*Ezh2*$^{\Delta/\Delta}$). Right: Immunoblotting in WT (JM8) and *Jarid2*$^{-/-}$ cells.

B. CLIP for Suz12 in *Ezh2*$^{fl/fl}$ (WT), *Ezh2*$^{\Delta/\Delta}$ and *Suz12*$^{-/-}$ cells, with and without UV crosslinking. Immunoblots for SUZ12 and EZH2 in the IPs are shown below.

C. Co-immunoprecipitation of EZH1 and EZH2 and β-actin (ACTB) by SUZ12 and control IgG in *Ezh2*$^{fl/fl}$ cells before and after treatment with Tmx to generate *Ezh2*$^{\Delta/\Delta}$ cells.

D. Co-immunoprecipitation of SUZ12 and EZH2 (and thus core PRC2) in WT and *Jarid2*$^{-/-}$ cells.

Supplemental Figure S6. Invariance of PRC2 RNA cross-linking in *Ezh2*$^{\Delta/\Delta}$ and *Jarid2*$^{-/-}$ cells.

A. Immunoblots for SUZ12 and EZH2 in the three *Ezh2*$^{\Delta/\Delta}$ cell samples used for iCLIP.

B. PRC2 crosslinks at (left) *Scl2a3* and *Enah* (right) in *Ezh2*$^{fl/fl}$, *Ezh2*$^{\Delta/\Delta}$, *Jarid2*$^{+/+}$ *and Jarid2*$^{-/-}$ cells. Details as for Figure 1B.

C. Scatter plot of PRC2 RNA significant crosslink density (RPKM) in WT (*Jarid2*$^{+/+}$) cells compared with *Jarid2*$^{-/-}$ cells.

D. MA plot showing the change in gene expression (RNA abundance) in *Ezh2*$^{\Delta/\Delta}$ cells compared with *Ezh2*$^{fl/fl}$ cells. RNAs showing a significant increase in abundance (used to generate Figure 4E) are coloured in red.

Supplemental Figure S7. Chromatin association of PRC2 subunits upon deletion of EZH2 or JARID2.

A. Immunofluorescence staining for SUZ12 and EZH2 in *Ezh2*$^{fl/fl}$ (WT), *Ezh2*$^{\Delta/\Delta}$ cells and *Jarid2*$^{-/-}$ cells. SUZ12 nuclear localization is maintained in the absence of EZH2. Scale bar corresponds to 50 μm.

B. ChIP-qPCR for PRC2-target genes and control genes in SUZ12, EZH2, H3K27me3, H3K27me1 and total H3 ChIPs from *Ezh2*$^{fl/fl}$ and *Ezh2*$^{\Delta/\Delta}$ cells, expressed as percentage input.

C. ChIP-qPCR for PRC2-target genes and control genes in SUZ12 and JARID2 ChIPs from *Jarid2*$^{+/+}$ and *Jarid2*$^{-/-}$ cells.

Supplemental Figure S8. Replicate experiments showing PRC2 RNA binding and chromatin association to be mutually antagonistic.

A. Replicate FUS and SUZ12 CLIP experiments in *Ezh2*$^{fl/fl}$ and *Ezh2*$^{\Delta/\Delta}$ cells. Details as for Figure 5C.

B. Replicate FUS and SUZ12 CLIP experiments in *Jarid2*$^{+/+}$ and *Jarid2*$^{-/-}$ cells. Details as for Figure 5D.

C. Replicate RNase A treatment experiments. Details as for Figure 6A.

D. Immunoblots for SUZ12 and H3 in chromatin (Chr), whole cell extract (Total), cytoplasmic and nucleoplasmic fractions from cells treated with RNase A or mock control for 15 and 30 minutes. 4% of each fraction was loaded, except for whole cell extract (1%). The exposure times for the chromatin and total fraction blot were 5s for H3 and 15s for SUZ12 and for the cytoplasmic and nucleoplasmic fraction blot the exposure times were 5 mins for H3 and 15 mins for SUZ12.

Supplemental Figure S9. PRC2 RNA binding antagonises chromatin association in cells.

A. Immunoblots for SUZ12 and H3 in the chromatin fraction of RNase A-treated cells before and after washing with PBS and incubation with yeast tRNA at 25, 12.5, 5, 1 and 0.2 μg/μl or with BSA at 2.5 μg/μl.

B. MNase chromatin digestion (0, 50, 100, 500, 2500 gel units/ml) of mock or RNase A-treated nuclei. No changes in chromatin accessibility were noted.

C. Left: Immunoblots for SUZ12, the Cohesin subunit RAD21 and H3 in *Rad21*$^{fl/fl}$ neural stem cells with or without addition of Tamoxifen to activate Cre-mediated recombination and with or without RNase A treatment. Right: Quantification of triplicate experiments. Unlike, RNase treatment, the deletion of *Rad21* and the subsequent loss of chromosomal architecture had no effect on SUZ12 chromatin association.

D. SUZ12 ChIP-seq read density (reads per million) at the *HoxA* locus following mock (black) or RNase A (red) treatment (2 replicates). PRC2 binding follows the expected pattern in both conditions.

E. Average EP300 chromatin binding profiles around gene TSS in mock (black) and RNase A (red) treated ESC. Genes are separated into active (nuclear and total RNA RPKM>1) and inactive (RPKM=0) and further divided by the presence or absence of a CpG island (CGI) at their TSS, as for Fig. 6D.

F. Average change in PRC2 binding upon RNase A treatment (left) or in cells overexpressing RNase H (right; data from (Chen et al. 2015)). Genes are divided into those at which PRC2 chromatin binding increases (red) or remains unchanged (blue) upon RNase A treatment. The increases in PRC2 chromatin interaction observed upon RNase A treatment are not observed in response to RNase H.

SUPPLEMENTAL TABLES

Supplemental Table S1. Numbers of RNA cross-linking events for each library at each stage of the filtering process.

Supplemental Table S2. Number of significant RNA crosslinks for each gene.

Supplemental Table S3. Genes at which PRC2 chromatin association is increased upon RNA degradation

Supplemental Figure S1

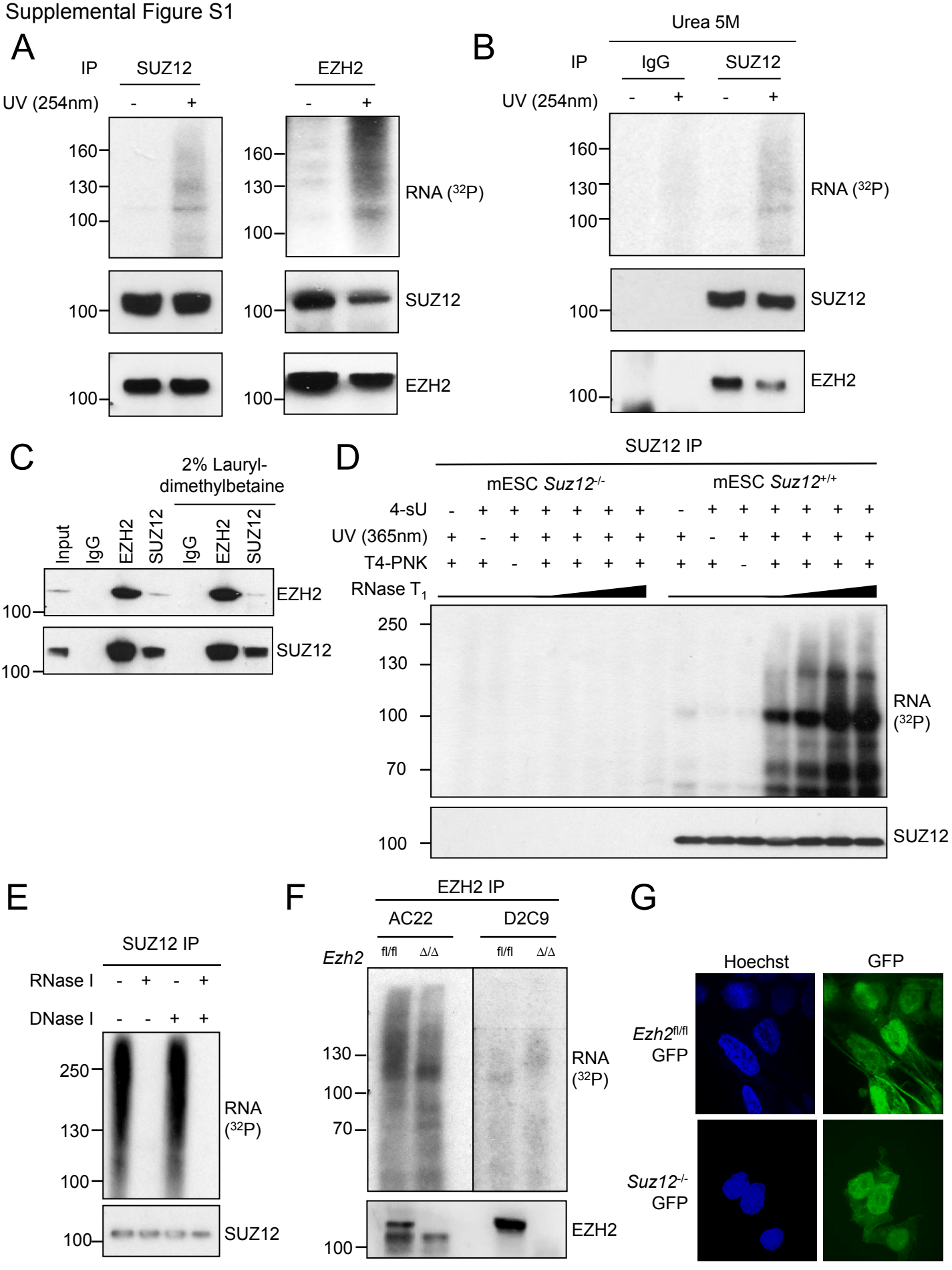

Supplemental Figure S2

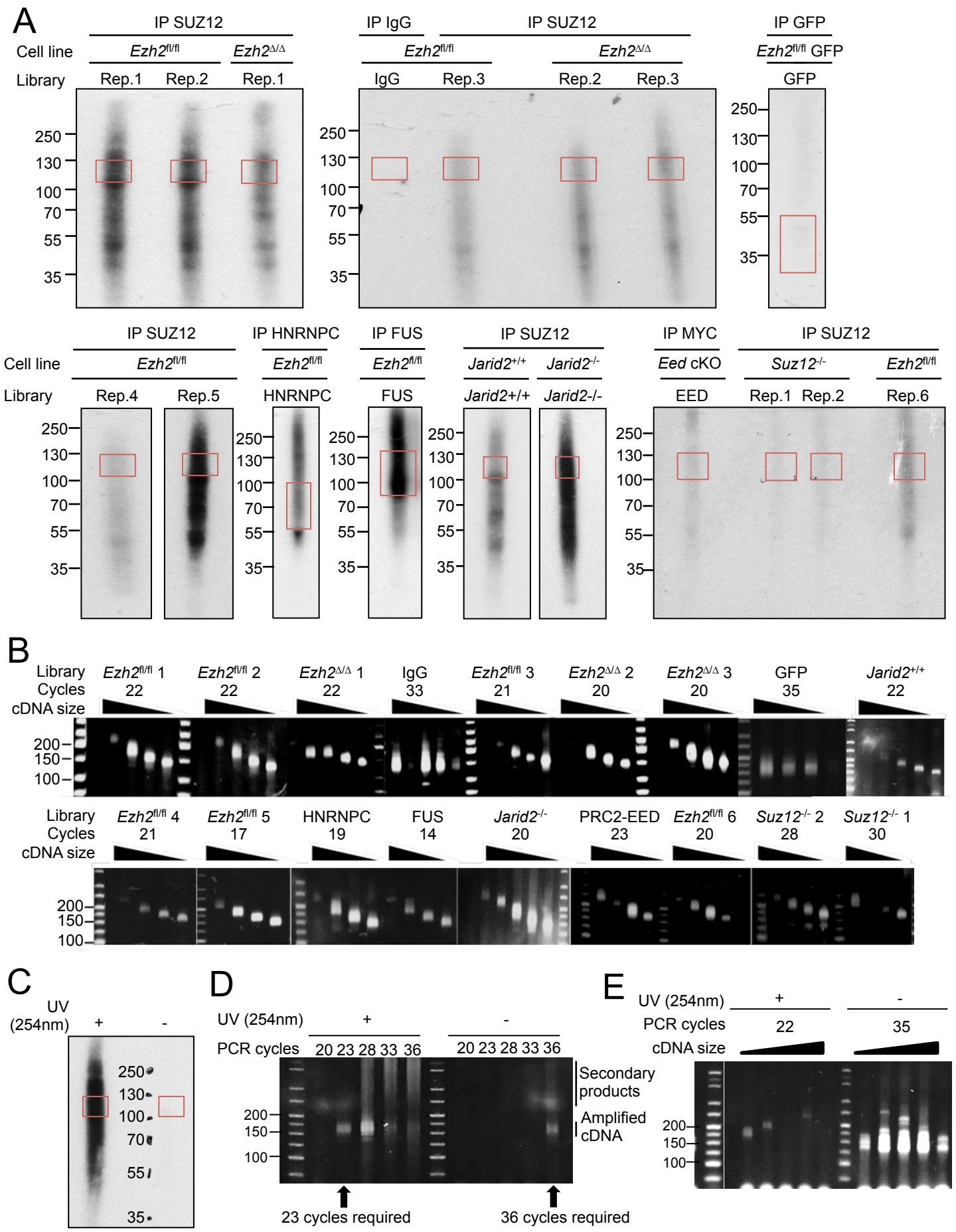

Supplemental Figure S3

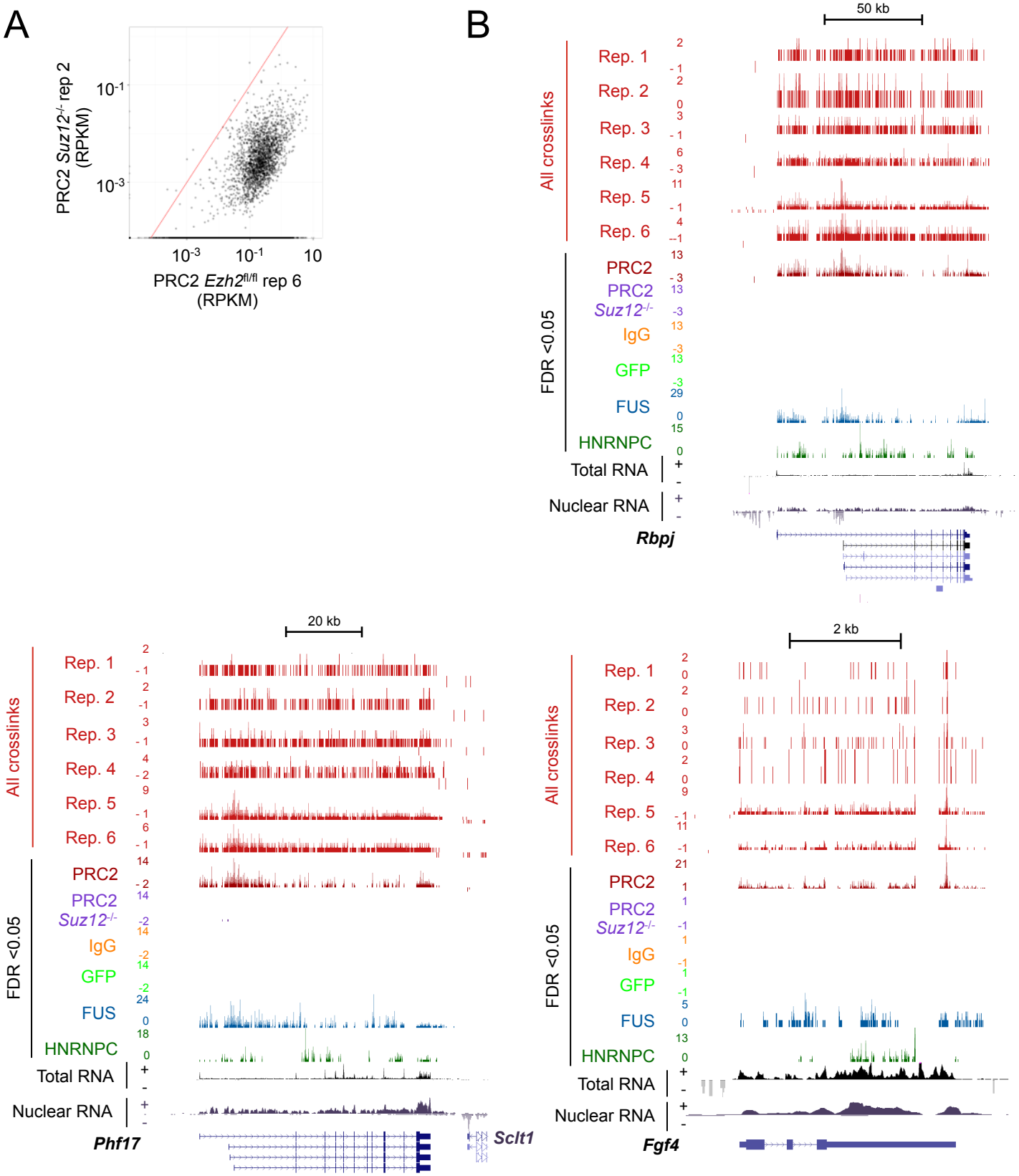

Supplemental Figure S4

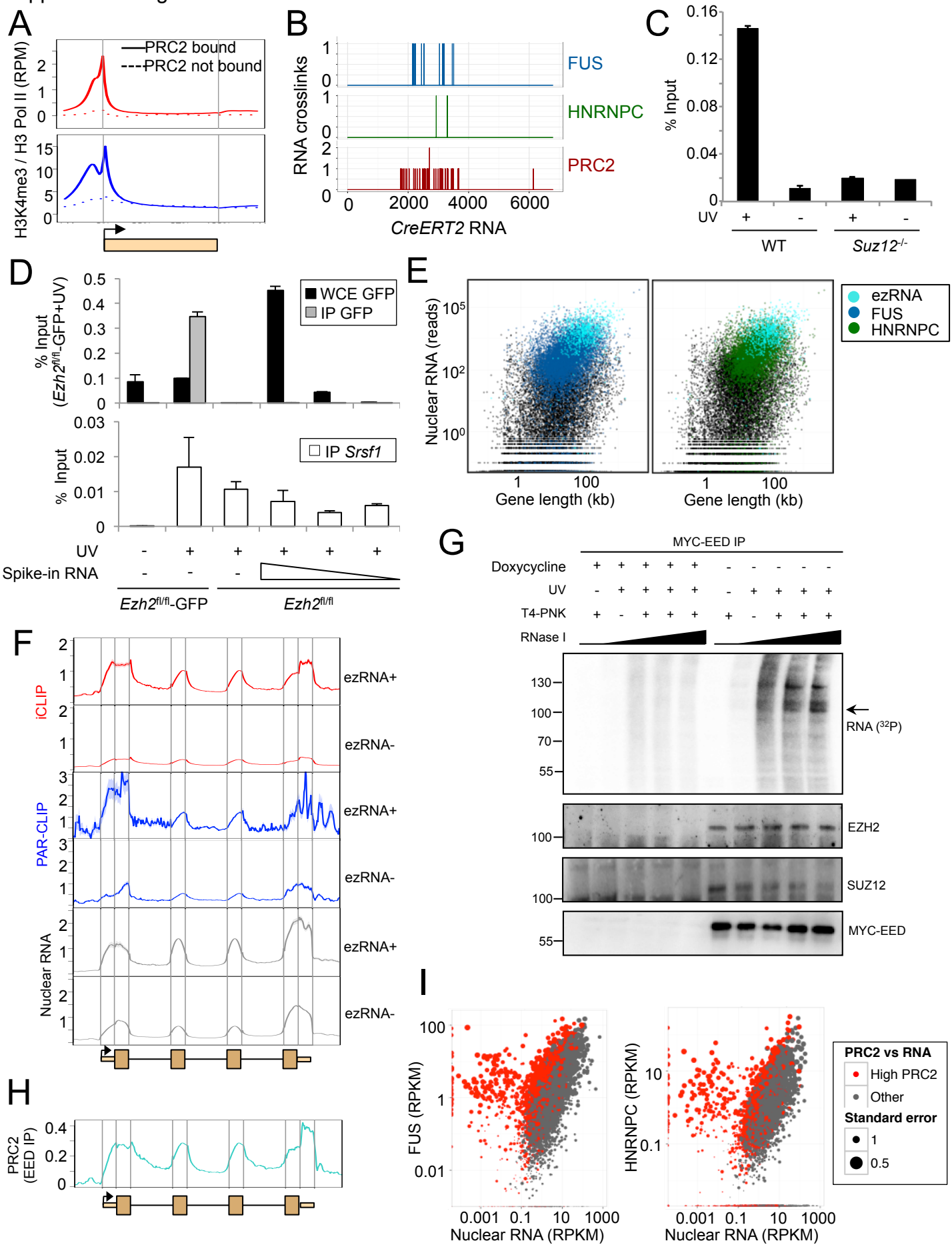

Supplemental Figure S5

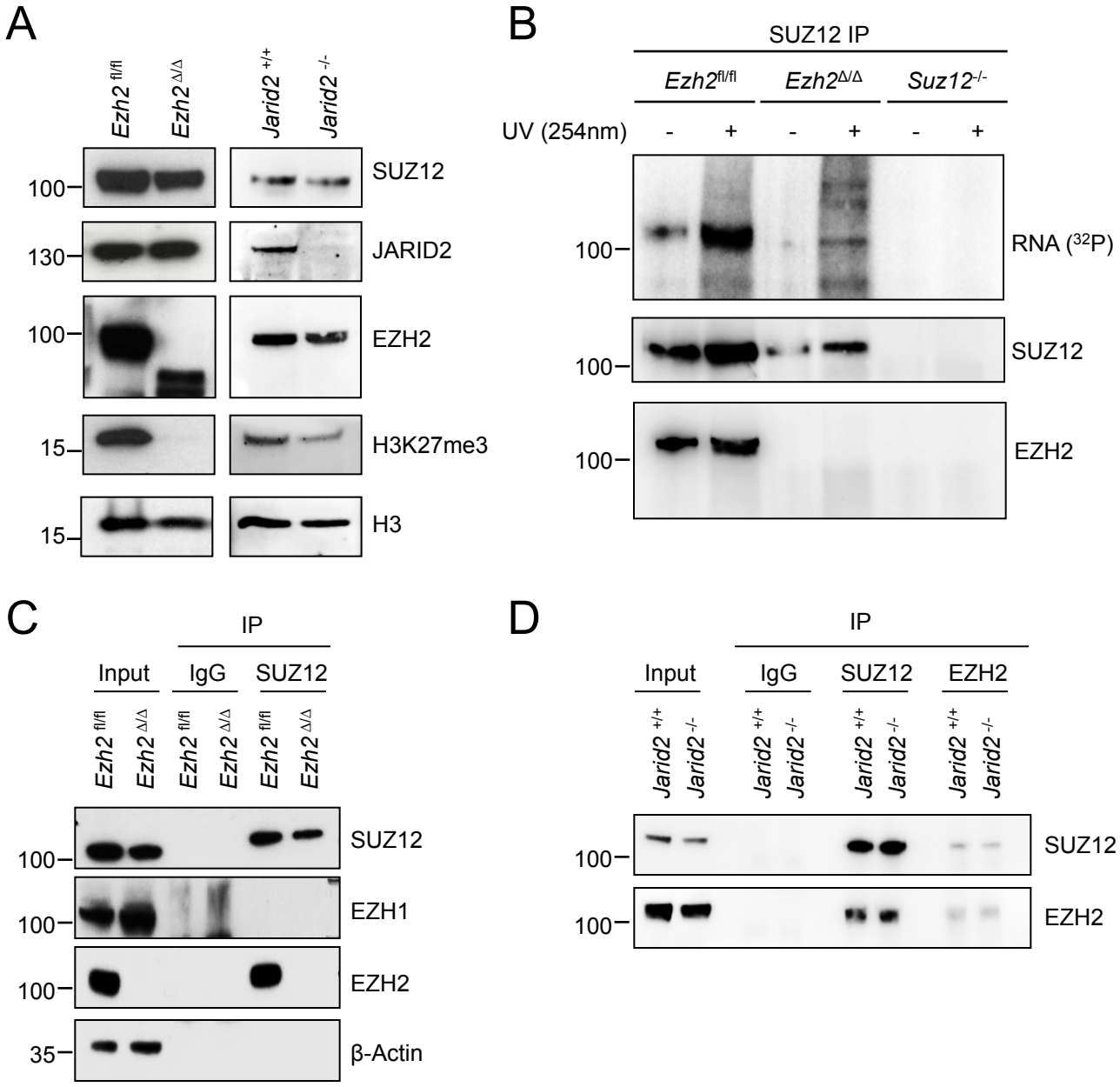

Supplemental Figure S6

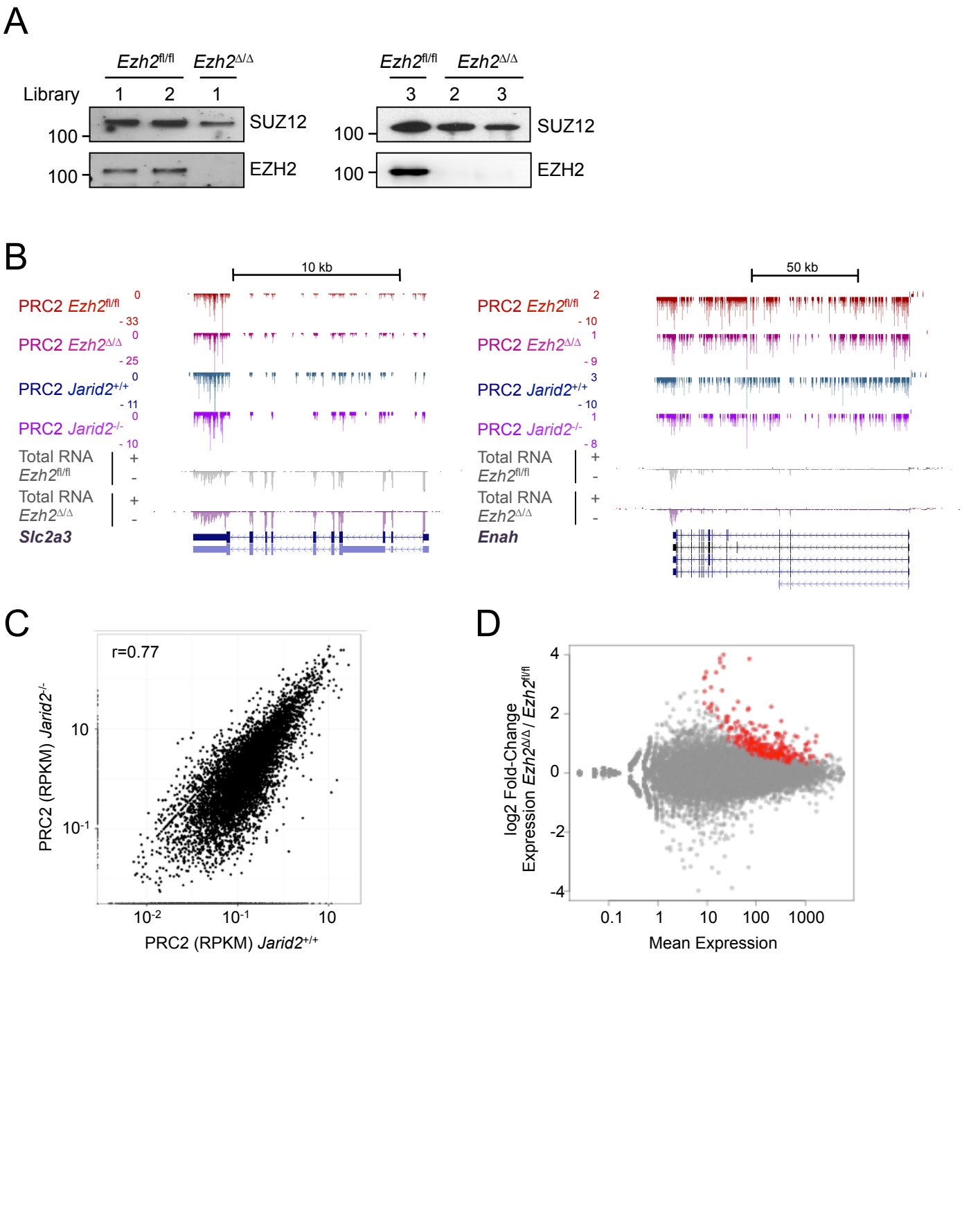

Supplemental Figure S7

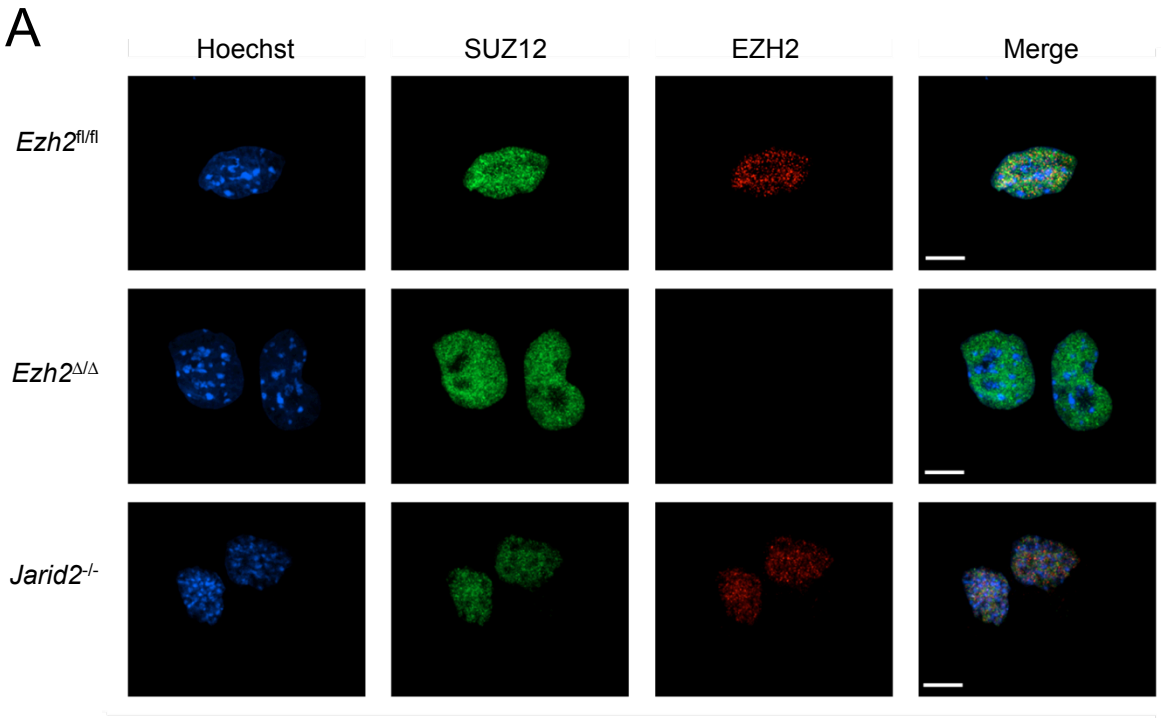

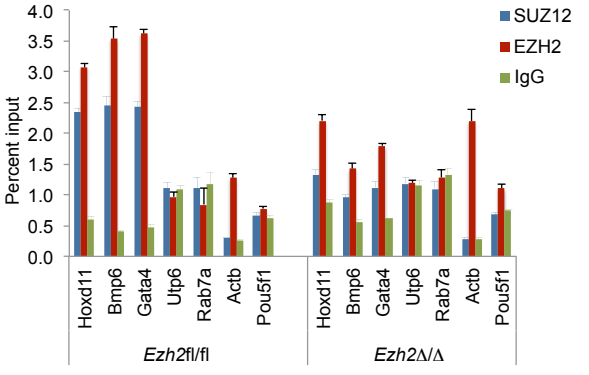

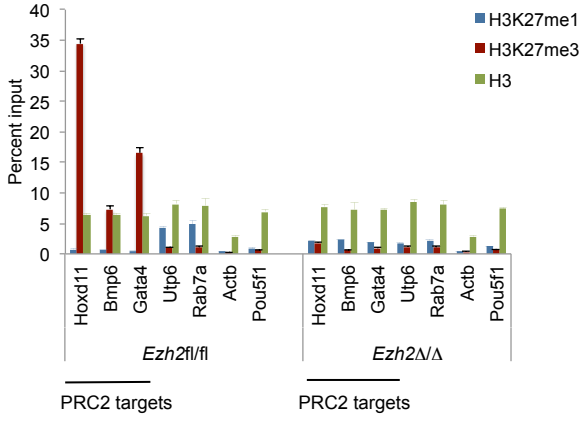

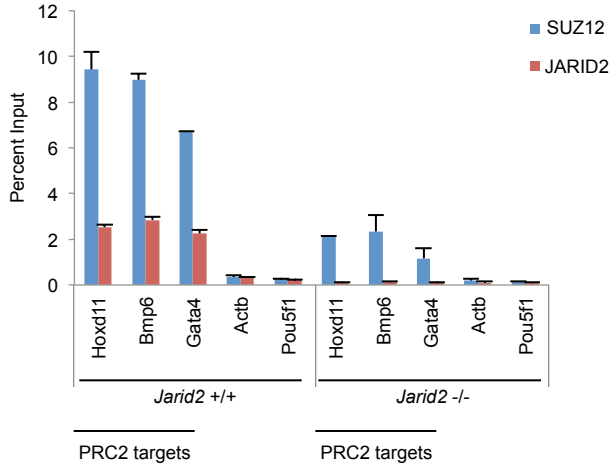

Supplemental Figure S8

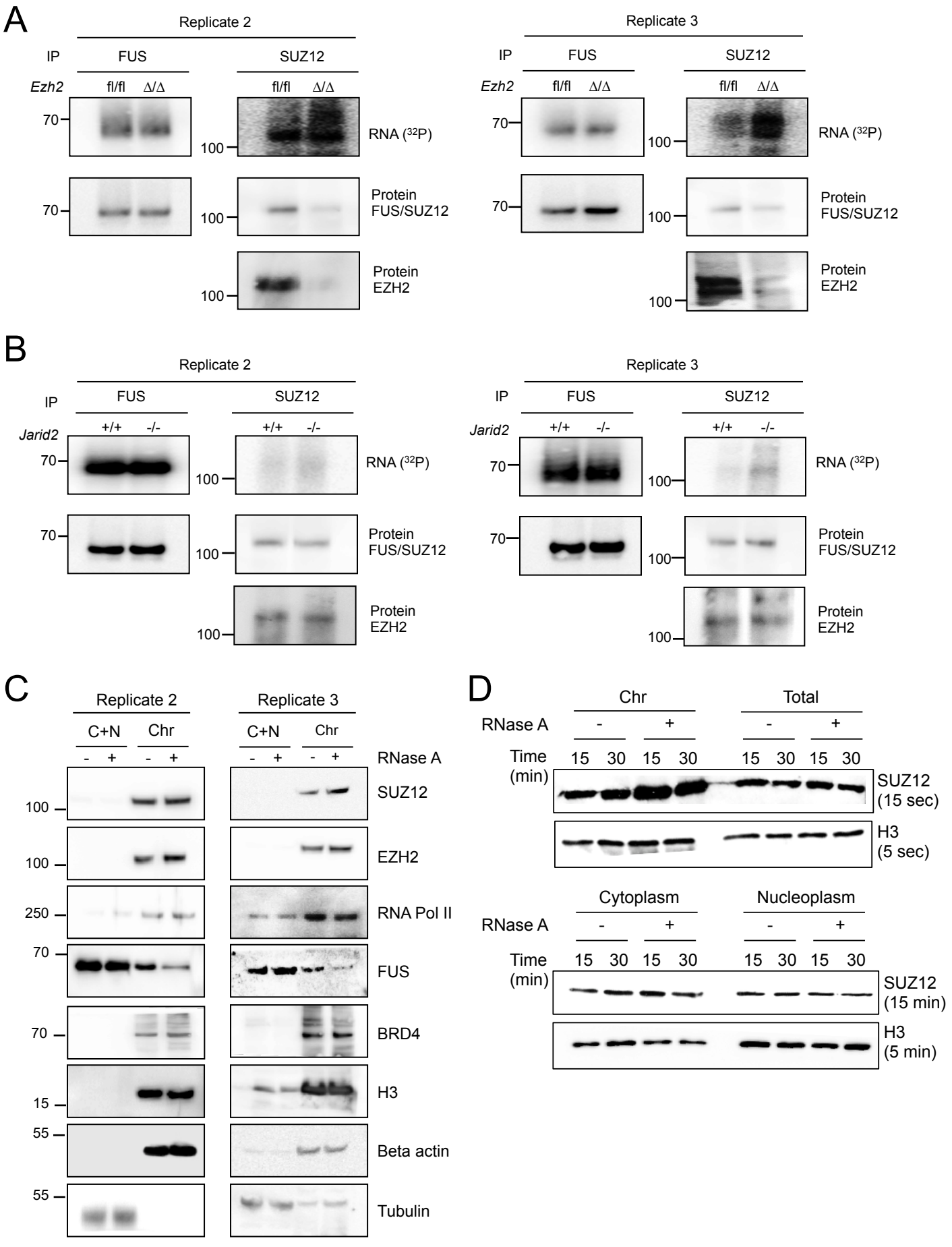

Supplemental Figure S9